

Light and Superlight Sterile Neutrinos in the Minimal Radiative Inverse Seesaw Model

P. S. Bhupal Dev and Apostolos Pilaftsis

*Consortium for Fundamental Physics, School of Physics and Astronomy,
University of Manchester, Manchester, M13 9PL, United Kingdom*

ABSTRACT

We explore the possibility of light and superlight sterile neutrinos in the recently proposed Minimal Radiative Inverse Seesaw extension of the Standard Model for neutrino masses, in which *all* existing neutrino data can be explained. In particular, we discuss two benchmark scenarios with one of the three sterile neutrino states in the keV-range, having very small mixing with the active neutrinos to account for the Dark Matter in the Universe, while (i) the other two light sterile neutrino states could be in the eV-range, possessing a nonzero mixing with the active states as required to explain the LSND+MiniBooNE+reactor neutrino data, or (ii) one of the light sterile states is in the eV-range, whereas the second one could be superlight and almost mass-degenerate with the solar neutrinos. Such superlight sterile neutrinos could give rise to potentially observable effects in future neutrino oscillation experiments and may also offer a possible explanation for the extra radiation observed in the Universe.

I. INTRODUCTION

A large number of solar, atmospheric, reactor and accelerator neutrino experiments provide solid pieces of evidence for the neutrino oscillation phenomenon, and hence for nonzero neutrino masses and mixing [1]. Most of these experimental results can be understood by oscillations of the three so-called *active* neutrinos, which appear in charged- and neutral-current weak interactions in the Standard Model (SM). A global fit [2, 3] to the three-neutrino oscillation data gives their best-fit mass-squared differences of $\Delta m_{\text{sol}}^2 = 7.5 \times 10^{-5} \text{ eV}^2$ and $\Delta m_{\text{atm}}^2 = 2.4 \times 10^{-3} \text{ eV}^2$. However, there are a few experimental results, most notably the LSND anomaly [4] and more recently the MiniBooNE results [5], as well as the reactor anti-neutrino anomaly [6], which cannot be explained within this three-neutrino-mixing paradigm and seem to require additional neutrino(s) with mass-squared differences of order 1 eV². Such additional neutrinos cannot couple directly to the SM Z -boson, due to the LEP constraint on its invisible decay width [7] which allows only three active light neutrinos. Hence, these neutrinos must be *sterile* neutrinos [8], i.e. SM gauge singlets, and can only participate in the SM weak interactions through their mixing with the active neutrinos.

In the light of recent predictions of a slightly higher reactor anti-neutrino flux [9], a global analysis of the short baseline (SBL) neutrino oscillation data favours the existence of more than one light sterile neutrino in the eV mass range [10–14]. On the other hand, cosmological data also indicate a weak preference for additional light degrees of freedom: $N_{\text{eff}} = 4.34 \pm 0.87$ [15], which could be interpreted as another evidence for sterile neutrinos in the eV/sub-eV mass range [14, 16].

The existence of light sterile neutrinos requires further theoretical justification, since unlike the active neutrinos, the sterile neutrino masses are not protected by the SM gauge symmetry. There are a number of interesting proposals in the literature [8]¹ to explain the lightness of the sterile neutrinos in various extensions of the SM, for nonzero active neutrino masses ν_{iL} (with $i = e, \mu, \tau$). In the simplest extension which realizes the type-I seesaw mechanism [18], n_R right-handed neutrinos $\nu_{\alpha R}$ (with $\alpha = 1, 2, \dots, n_R$) are added to the SM some of which could in principle play the role of light sterile neutrinos, provided their masses are in the eV range [19]. The masses and mixing of the active and sterile neutrinos can be deduced from the $(3 + n_R) \times (3 + n_R)$ complex symmetric neutrino mass matrix in the flavour

¹ Light sterile neutrinos can also occur in theories of quantum gravity due to gravitational interactions involving global anomalies related to quantum torsion [17].

basis $\{(\nu_{iL})^C, \nu_{\alpha R}\}$:

$$\mathcal{M}_\nu = \begin{pmatrix} \mathbf{0} & M_D \\ M_D^\top & M_R \end{pmatrix}, \quad (1)$$

where M_D is the Dirac neutrino mass matrix, and M_R is the $(B - L)$ -breaking Majorana mass matrix of the singlet neutrinos. In the usual seesaw approximation $\|\xi\| \equiv \|M_D M_R^{-1}\| \ll 1$, with $\|\xi\| \equiv \sqrt{\text{Tr}(\xi^\dagger \xi)}$ being the norm of the matrix ξ , the light neutrino masses are determined from the mass matrix

$$M_{\nu L} \simeq -M_D M_R^{-1} M_D^\top, \quad (2)$$

with mass eigenvalues $m_{1,2,3}$, whereas the heavier masses are roughly the eigenvalues of M_R : $m_{4,5,\dots,3+n_R} \gg m_{1,2,3}$. In this case, the active-sterile mixing, given by $\Theta \sim (m_{1,2,3}/m_{4,5,\dots,n_R})^{1/2}$, is very small, thus limiting our ability to observe the singlet neutrinos, unless $M_R \lesssim 10$ eV which are mostly excluded over a wide range by the present data [20].

It is therefore interesting to examine a theoretical framework yielding simultaneously light sterile neutrinos as favoured by the SBL neutrino oscillation data and a sizable active-sterile mixing to be observable in the current or near future experiments. An attractive possibility is the so-called inverse seesaw model [21], where in addition to the right-handed neutrinos as in the type-I seesaw model, another set of SM singlet fermions $S_{\rho L}$ (with $\rho = 1, 2, \dots, n_S$) is introduced. In this case, the mass matrix in (1) gets extended to the following $(3 + n_R + n_S) \times (3 + n_R + n_S)$ general mass matrix in the basis $\{(\nu_{iL})^C, \nu_{\alpha R}, (S_{\rho L})^C\}$:

$$\mathcal{M}_\nu = \begin{pmatrix} \mathbf{0} & M_D & \mathbf{0} \\ M_D^\top & \mu_R & M_N^\top \\ \mathbf{0} & M_N & \mu_S \end{pmatrix}, \quad (3)$$

where in addition to the usual Dirac mass matrix M_D and the Majorana mass matrix μ_R in the ν_L - ν_R sector, we have added another Dirac mass matrix M_N and Majorana mass matrix μ_S in the ν_R - S singlet sector. Observe that the standard inverse seesaw model discussed originally in [21] is recovered, once we set the right-handed neutrino Majorana mass $\mu_R = \mathbf{0}$ in (3). In this case, for $\|\mu_S\| \ll \|M_N\|, \|M_D\|$, it is possible to have very light sterile neutrinos, e.g. in the presence of a $\mu - \tau$ symmetry [22] or in theories with warped extra dimensions [23].

Another interesting realization of inverse seesaw models arises, when $\mu_R \neq \mathbf{0}$, but $\mu_S = \mathbf{0}$ ². In this case, the rank of the mass matrix given by (3) reduces to $3 + n_R$, and the light neutrinos are *exactly* massless at the tree level. However, they acquire a small mass at the one-loop level which is *directly* proportional to the Majorana mass matrix μ_R [25] and results from well-known SM radiative corrections involving the Z - and Higgs bosons [26]. This scenario, called the Minimal Radiative Inverse Seesaw Model (MRISM) in [25], is very economical, as it does not require the existence of other non-standard scalar or gauge fields or other fermionic matter beyond the singlet neutrinos $\{\nu_{\alpha R}, S_{\rho L}\}$.

In this paper, we study the possibility of having light sterile neutrinos in the MRISM with three pairs of singlet neutrinos $\{\nu_{iL}, S_{\rho L}\}$ (for $i, \rho = 1, 2, 3$). In the limit $\|\mu_R\| \gg \|M_D\|, \|M_N\|$, after integrating out the three heavy singlet states $\nu_{1,2,3R}$ with masses of order $\|\mu_R\|$, we are left with six light mass states. Of these six light states, three should describe the mostly active neutrinos and the remaining three will be mostly sterile states. In particular, we discuss two benchmark scenarios. In the first scenario, all the sterile neutrinos are heavier than the active ones, with two of them having mass in the eV-range (as in the 3+2 models) to explain the LSND+MiniBooNE+reactor data, while the remaining one is in the keV-range to account for the Dark Matter (DM) in the Universe [27]. In the second scenario, one of the sterile neutrinos is in the keV-range as in the first scenario, and the second one is in the eV-range (as in the 3+1 models), while the third sterile neutrino is *superlight* and almost mass-degenerate with the electron neutrino ν_{eL} . We present numerical estimates of the model parameters for both of these benchmark scenarios. Finally, we also comment on another possibility discussed in the literature when all the three sterile states are in the eV-range (the 3+3 models).

² This structure may arise, for instance, in models where the Majorana masses for the S -fields are forbidden due to specific flavour symmetries [24].

The paper is organized as follows. In Section II, we briefly review the MRISM and present the effective neutrino mass matrix after integrating out the heavy sterile states. In Section III, we analyze the simple case of one single flavour, for illustration purposes. In Section IV, we generalize our analysis to the three flavour case and discuss the experimental constraints on the mixing parameters. In Section V, we present our results for the benchmark scenarios mentioned above. Our conclusions are given in Section VI. In Appendix A, we give a general parametrization of the unitary matrix used in our analysis.

II. STERILE NEUTRINOS IN THE MRISM

In the limit $\|\mu_R\| \gg \|M_D\|, \|M_N\|$, the ν_R -fields decouple below the mass scale μ_R , resulting in an effective theory with six neutrino states: $\nu_{e,\mu,\tau L}$ and $S_{1,2,3L}$. At the tree level, the effective neutrino mass matrix in the weak basis $\{\nu_{e,\mu,\tau L}, S_{1,2,3L}\}$ becomes

$$\mathcal{M}_{\text{eff}}^{\text{tree}} = \begin{pmatrix} M_D \mu_R^{-1} M_D^T & M_D \mu_R^{-1} M_N^T \\ M_N \mu_R^{-1} M_D^T & M_N \mu_R^{-1} M_N^T \end{pmatrix} = \begin{pmatrix} M_D \\ M_N \end{pmatrix} \mu_R^{-1} \begin{pmatrix} M_D^T & M_N^T \end{pmatrix}. \quad (4)$$

Note that one of the block eigenvalues must vanish, since the effective mass matrix $\mathcal{M}_{\text{eff}}^{\text{tree}}$ has rank 3. The matrix $\mathcal{M}_{\text{eff}}^{\text{tree}}$ can be block-diagonalized by a unitary transformation:

$$\mathcal{V}^T \mathcal{M}_{\text{eff}}^{\text{tree}} \mathcal{V} = \begin{pmatrix} \mathbf{0}_3 & \mathbf{0}_3 \\ \mathbf{0}_3 & M \mu_R^{-1} M^T \end{pmatrix}, \quad (5)$$

where the unitary matrix \mathcal{V} has an exact representation in terms of an arbitrary matrix ζ [28]:

$$\mathcal{V} = \begin{pmatrix} (\mathbf{1}_3 + \zeta^* \zeta^T)^{-1/2} & \zeta^* (\mathbf{1}_3 + \zeta^T \zeta^*)^{-1/2} \\ -\zeta^T (\mathbf{1}_3 + \zeta^* \zeta^T)^{-1/2} & (\mathbf{1}_3 + \zeta^T \zeta^*)^{-1/2} \end{pmatrix}. \quad (6)$$

From (5), it is straightforward to obtain

$$\zeta = M_D M_N^{-1} \quad \text{and} \quad M = (\mathbf{1}_3 + \zeta^\dagger \zeta)^{1/2} M_N. \quad (7)$$

At the one-loop level, the mass matrix given by (4) receives an electroweak radiative correction proportional to μ_R [25], which in the limit $\|\mu_R\| \gg \|M_D\|, \|M_N\|$ is given by

$$\begin{aligned} \mathcal{M}_{\text{eff}}^{1\text{-loop}} &\simeq \begin{pmatrix} M_D \\ \mathbf{0}_3 \end{pmatrix} \frac{\alpha_W}{16\pi m_W^2} \mu_R \left[\frac{m_H^2}{\mu_R^2 - m_H^2} \mathbf{1}_3 \ln \left(\frac{\mu_R^2}{m_H^2} \right) + \frac{3m_Z^2}{\mu_R^2 - m_Z^2} \mathbf{1}_3 \ln \left(\frac{\mu_R^2}{m_Z^2} \right) \right] \begin{pmatrix} M_D^T & \mathbf{0}_3 \end{pmatrix} \\ &= \begin{pmatrix} M_D \mu_R^{-1} x_R f(x_R) M_D^T & \mathbf{0}_3 \\ \mathbf{0}_3 & \mathbf{0}_3 \end{pmatrix} \equiv \begin{pmatrix} \Delta M & \mathbf{0}_3 \\ \mathbf{0}_3 & \mathbf{0}_3 \end{pmatrix}, \end{aligned} \quad (8)$$

where the one-loop function $f(x_R)$ is defined as

$$f(x_R) = \frac{\alpha_W}{16\pi} \left[\frac{x_H}{x_R - x_H} \ln \left(\frac{x_R}{x_H} \right) + \frac{3x_Z}{x_R - x_Z} \ln \left(\frac{x_R}{x_Z} \right) \right] \quad (9)$$

with $x_R \equiv \hat{\mu}_R^2/m_W^2$, $x_H \equiv m_H^2/m_W^2$, $x_Z \equiv m_Z^2/m_W^2$, assuming $\mu_R = \hat{\mu}_R \mathbf{1}_3$ for simplicity. The functions $f(x_R)$ and $x_R f(x_R)$ are plotted in Fig. 1.

Thus, the full neutrino mass matrix in the basis $\{\nu_{e,\mu,\tau L}, S_{1,2,3L}\}$ is given by

$$\mathcal{M}_{\text{eff}} = \mathcal{M}_{\text{eff}}^{\text{tree}} + \mathcal{M}_{\text{eff}}^{1\text{-loop}} = \begin{pmatrix} M_D \mu_R^{-1} (\mathbf{1}_3 + x_R f(x_R)) M_D^T & M_D \mu_R^{-1} M_N^T \\ M_N \mu_R^{-1} M_D^T & M_N \mu_R^{-1} M_N^T \end{pmatrix}. \quad (10)$$

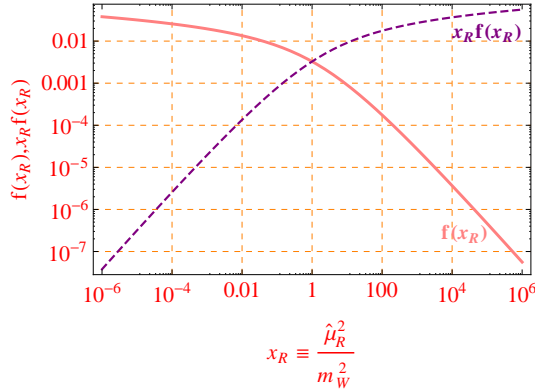


FIG. 1: The analytic dependence of the one-loop function $f(x_R)$ and $x_R f(x_R)$ on the Majorana mass scale $\hat{\mu}_R$.

Since the loop-function $x_R f(x_R)$ is much smaller than unity for a wide range of $\hat{\mu}_R$ as shown in Fig. 1, we can use the unitary matrix \mathcal{V} given by (6) to perturbatively block-diagonalize the full mass matrix in (10), as follows:

$$\begin{aligned} \mathcal{V}^\top \mathcal{M}_{\text{eff}} \mathcal{V} &= \begin{pmatrix} (\mathbf{1}_3 + \zeta \zeta^\dagger)^{-1/2} \Delta M (\mathbf{1} + \zeta^* \zeta^\top)^{-1/2} & (\mathbf{1}_3 + \zeta \zeta^\dagger)^{-1/2} \Delta M \zeta^* (\mathbf{1} + \zeta^\top \zeta^*)^{-1/2} \\ (\mathbf{1}_3 + \zeta^\dagger \zeta)^{-1/2} \zeta^\dagger \Delta M (\mathbf{1} + \zeta^* \zeta^\top)^{-1/2} & M \mu_R^{-1} M^\top + (\mathbf{1}_3 + \zeta^\dagger \zeta)^{-1/2} \zeta^\dagger \Delta M \zeta^* (\mathbf{1} + \zeta^\top \zeta^*)^{-1/2} \end{pmatrix} \\ &\equiv \begin{pmatrix} m_{11} & m_{12} \\ m_{12}^\top & M \mu_R^{-1} M^\top + m_{22} \end{pmatrix}. \end{aligned} \quad (11)$$

Since $\|m_{12}\|, \|m_{22}\| \ll \|M \mu_R^{-1} M^\top\|$, we can make the usual seesaw-like approximation to obtain the block mass eigenvalues:

$$M_1 \simeq m_{11} - m_{12} (M \mu_R^{-1} M^\top)^{-1} m_{12}^\top, \quad (12)$$

$$M_2 \simeq M \mu_R^{-1} M^\top. \quad (13)$$

It is clear from (12) that the light neutrino mass block eigenvalue is proportional to the loop-correction factor ΔM , and vanishes as $\Delta M \rightarrow \mathbf{0}$. Note that the second term in (12) represents an effective two-loop effect of $\mathcal{O}((\Delta M)^2)$, and next to the first term, it can be safely ignored.

In order to obtain the active and sterile components for each mass eigenvalue, the mass matrix in (11) needs to be further diagonalized into a fully mass-diagonal form. Before doing so for the general three-flavour scenario in Section IV, we will first consider a simple one-flavour scenario for illustration purposes, which would help us to gain valuable insight.

III. THE SINGLE FLAVOUR CASE

In this case, we replace all the matrices in (12) and (13) by complex numbers. Then, the mass eigenvalues are simply given by

$$m_1 = \frac{x_R f(x_R) m_N^2}{\hat{\mu}_R} \left(\frac{\zeta^2}{1 + |\zeta|^2} \right), \quad m_2 = \frac{m_N^2}{\hat{\mu}_R} (1 + |\zeta|^2), \quad (14)$$

while the mass eigenvectors are given by

$$\begin{pmatrix} n_1 \\ n_2 \end{pmatrix} = \mathcal{V}^\dagger \begin{pmatrix} \nu_L \\ \nu_S \end{pmatrix} = (1 + |\zeta|^2)^{-1/2} \begin{pmatrix} \nu_L - \zeta^* S_L \\ \zeta \nu_L + S_L \end{pmatrix}. \quad (15)$$

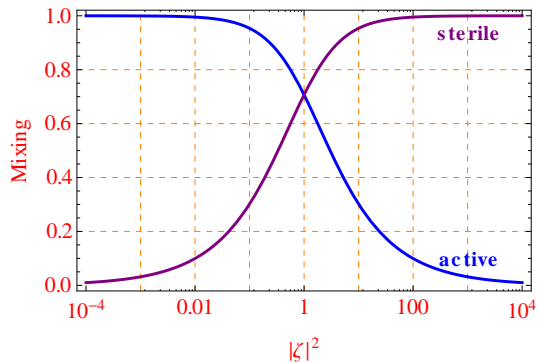


FIG. 2: The active and sterile components in the lighter neutrino state n_1 defined in (15) for the single flavour case.

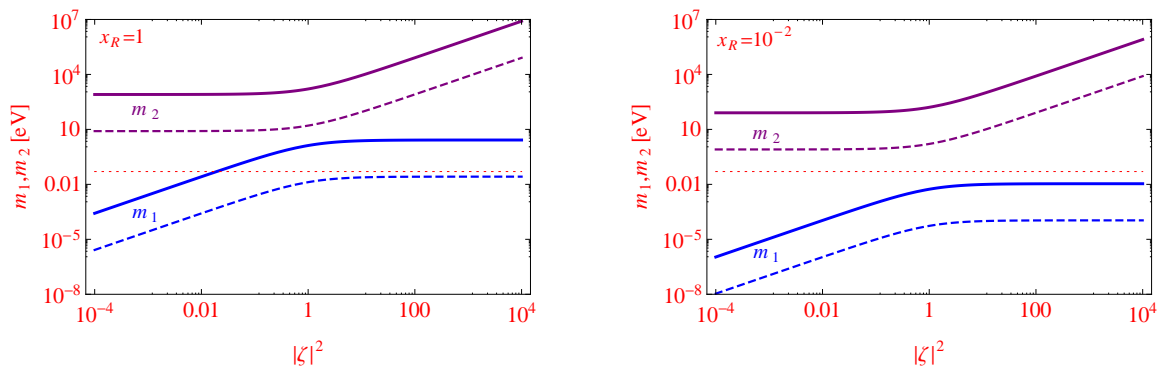


FIG. 3: The light neutrino mass eigenvalues m_1 and m_2 for the single flavour case with two different choices of $x_R = \mu_R^2/m_W^2$ and with $|m_N| = 10^{-4}\mu_R$ (solid), $10^{-5}\mu_R$ (dashed). The horizontal red (dotted) line represents the tentative upper limit on the active neutrino mass scale.

From (15), we note that in the limit $\|\zeta\| \ll 1$, the massless state is mostly the active neutrino ν_L , whereas in the limit $\|\zeta\| \gg 1$, the massless state is mostly the sterile neutrino S_L . This generic property is illustrated in Fig. 2.

The magnitudes of these eigenvalues are shown in Fig. 3, as a function of $|\zeta|^2$ for two typical values of the Majorana mass scale $\mu_R = x_R m_W^2$. In each case, we show the values for two choices of $|m_N|/\mu_R = 10^{-4}, 10^{-5}$, given by the solid and dashed lines, respectively. The dotted horizontal line shows the experimental upper limit on the active neutrino mass, assuming a normal hierarchy with vanishing ν_e mass. From Fig. 3 we see that even in this simple scenario, it is possible to have a sterile neutrino in the keV-mass range to be a DM candidate (for $|m_N|/\mu_R \gtrsim 10^{-4}$) or in the eV-range to explain the LSND anomaly (for $|m_N|/\mu_R \lesssim 10^{-5}$). In both the cases, we must have $|\zeta|^2 \ll 1$, so that the lighter mass eigenstate is mostly the active neutrino (cf. Fig. 2) with mass in the sub-eV range.

IV. THE THREE FLAVOUR CASE

We now turn our attention to the general case with three active neutrinos (ν_e, ν_μ, ν_τ) and three light sterile neutrinos ($\nu_{s_1}, \nu_{s_2}, \nu_{s_3}$). In this case, we diagonalize the full 6×6 light neutrino mass matrix in (10) by a general unitary matrix \mathcal{U}_6 :

$$\mathcal{M}_{\text{eff}} = \mathcal{U}_6^* \begin{pmatrix} \widehat{M}_{123} & \mathbf{0}_3 \\ \mathbf{0}_3 & \widehat{M}_{456} \end{pmatrix} \mathcal{U}_6^\dagger, \quad (16)$$

where $\widehat{M}_{123} = \text{diag}(m_1, m_2, m_3)$ and $\widehat{M}_{456} = \text{diag}(m_4, m_5, m_6)$, with $m_{1,\dots,6}$ being the mass eigenvalues of \mathcal{M}_{eff} . Moreover,

$$\mathcal{U}_6 = \begin{pmatrix} U_{e1} & U_{e2} & U_{e3} & U_{e4} & U_{e5} & U_{e6} \\ U_{\mu1} & U_{\mu2} & U_{\mu3} & U_{\mu4} & U_{\mu5} & U_{\mu6} \\ U_{\tau1} & U_{\tau2} & U_{\tau3} & U_{\tau4} & U_{\tau5} & U_{\tau6} \\ U_{s11} & U_{s12} & U_{s13} & U_{s14} & U_{s15} & U_{s16} \\ U_{s21} & U_{s22} & U_{s23} & U_{s24} & U_{s25} & U_{s26} \\ U_{s31} & U_{s32} & U_{s33} & U_{s34} & U_{s35} & U_{s36} \end{pmatrix} \quad (17)$$

is a 6×6 unitary matrix that relates the flavour states $\{\nu_e, \nu_\mu, \nu_\tau, \nu_{s_1}, \nu_{s_2}, \nu_{s_3}\}$ to the mass eigenstates $\{\nu_1, \nu_2, \dots, \nu_6\}$.

As shown in Appendix A, \mathcal{U}_6 can be parametrized in terms of 15 Euler angles and 10 Dirac phases³. This, together with the six mass eigenvalues, introduces a total of 31 parameters on the right-hand-side of (16) some of which can be constrained experimentally, as follows. The only experimentally measured neutrino parameters so far are the three mixing angles $\theta_{12}, \theta_{23}, \theta_{13}$ between the mostly active neutrinos, and the two mass-squared differences Δm_{21}^2 and Δm_{31}^2 [1]. Also, there is some hint for a nonzero Dirac CP phase φ_{13} from the global analysis of the 3-neutrino data [2, 3]. For our numerical analysis, we use the latest best-fit values of these parameters as given in [2], taking into account the reactor SBL data and assuming a normal hierarchy:

$$\begin{aligned} \theta_{12} &= 33.3^\circ, & \theta_{23} &= 40.0^\circ, & \theta_{13} &= 8.6^\circ, & \varphi_{13} &= 1.67\pi, \\ \Delta m_{21}^2 &= 7.50 \times 10^{-5} \text{ eV}^2, & \Delta m_{31}^2 &= 2.47 \times 10^{-3} \text{ eV}^2. \end{aligned} \quad (18)$$

On the other hand, for the mass and mixing parameters involving the sterile sector, there has been a number of recent analyses [10–14] involving one, two and three sterile neutrinos, denoted as (3+1), (3+2) and (3+3)-scenarios respectively. Although their global best-fit values for any particular scenario differ somewhat from each other, they all agree on the conclusion that there is a strong tension in the global data for the (3+1)-scenario [8, 29]. This is mainly because the neutrino versus anti-neutrino and appearance versus disappearance data sets prefer two different values of Δm_{41}^2 for the (3+1)-scenario [13]. The neutrino versus anti-neutrino discrepancy is somewhat reduced in the (3+2)- and (3+3)-scenarios due to the additional CP -violating phases, thus leading to better global fits. However, the appearance versus disappearance tension still remains, and in particular, the fit to the latest MiniBooNE low-energy data is not improved by adding more sterile neutrinos. Thus due to the lack of a clear preference at the moment, we will consider benchmark cases for our model using both (3+1)- and (3+2)-fits, and will also comment on the (3+3)-fit.

There also exist upper bounds on the absolute neutrino mass scale which could in principle be used to constrain the masses of the light sterile neutrinos and their mixing with the active ones. These constraints are briefly summarized below:

1. The effective neutrino mass parameter in β -decay experiments:

$$m_\beta = \sqrt{\sum_i |U_{ei}|^2 m_i^2}, \quad (19)$$

which determines the distortion of the electron energy spectrum due to nonzero neutrino mass and mixing. The current most stringent upper limit on this parameter is $m_\beta \leq 2.2 \text{ eV}$ [30, 31], which is still compatible with the entire favoured region of the global fits [32]. The upcoming KATRIN experiment [33] with estimated sensitivity reach, as low as 0.2 eV, should be able to probe a substantial fraction of the allowed parameter space [34].

2. The effective neutrino mass parameter in neutrinoless double beta decay ($0\nu\beta\beta$) experiments:

$$\langle m \rangle_{\beta\beta} = \left| \sum_i U_{ei}^2 m_i \right| = \left| \sum_i |U_{ei}|^2 e^{i\alpha_i} m_i \right|, \quad (20)$$

³ For simplicity, we set all Majorana phases to zero.

where α_i are the Majorana phases associated with the elements U_{ei} . The strongest bound so far on $\langle m \rangle_{\beta\beta} < 0.26$ eV [35–38] and significant improvements are expected to take place in the near future [39]. However, since the Majorana phases in (20) are still unknown, it is possible to have cancellations among them [40], and hence, the constraint on $\langle m \rangle_{\beta\beta}$ may not apply for the sterile neutrino sector. For our benchmark model parameters discussed in Section V, the $0\nu\beta\beta$ contribution from the sterile sector is known to be negligible [41].

3. The sum of the neutrino masses, $\sum_i m_i$, contributing to the total energy density in our Universe. This parameter can be constrained from the analysis of data on several cosmological observables [42], and the current upper limits are in the eV range which are in tension with the sterile neutrino-favored region of the SBL data. The cosmologically-derived bounds, however, depend on the assumptions made on the cosmic history of the early Universe, as well as on the corresponding cosmological data set used, besides the uncertainties associated with the observables [14, 16, 43]. It might be possible to resolve some of these issues by analyzing the upcoming galaxy survey data [44]. It might also be plausible to consider a deviation from the standard cosmological picture, in order to accommodate the eV-scale sterile neutrinos as favoured by the SBL data [8]. A proper analysis of this possibility is beyond the scope of this paper. Hence, we do not consider the cosmological bounds for the rest of our discussion.

In addition, the constraints on the active-sterile mixing from the non-unitarity of the PMNS mixing matrix [45] need to be taken into account as well. In the inverse seesaw model with $\mu_R = \mathbf{0}$ and $\mu_S \neq \mathbf{0}$, the non-unitarity effects are proportional to $\|\zeta\|^2$ [46]. For the MRISM with $\mu_R \neq \mathbf{0}$ and $\mu_S = \mathbf{0}$, the non-unitarity effects due to the mixing between the active and heavy sterile neutrinos in (3) is of order $\|M_D\mu_R^{-1}\|^2$ which, as we will see in the following section, is very small ($\sim 10^{-9}$). This justifies our diagonalization procedure in (16) using a unitary matrix \mathcal{U}_6 . With the parametrization of \mathcal{U}_6 as given in Appendix A, the non-unitarity due to the mixing between the active and light sterile neutrinos is determined by RR^\dagger [cf. (A7)]. Using a combination of neutrino oscillation data and unitarity constraints in weak decays, the following allowed ranges for $|V|$ have been derived [45]:

$$|V| = \begin{pmatrix} 0.75 - 0.89 & 0.45 - 0.65 & < 0.20 \\ 0.19 - 0.55 & 0.42 - 0.74 & 0.57 - 0.82 \\ 0.13 - 0.56 & 0.36 - 0.75 & 0.54 - 0.82 \end{pmatrix}. \quad (21)$$

However, the constraints derived from weak decays are not directly applicable for the sterile neutrino masses below the electroweak scale as in our case. Also the constraints from Lepton Flavour Universality which may lead to measurable enhancements in various flavour physics observables [47] are not applicable to our case with all the light sterile masses much below the MeV scale. We find that the numerical values of the active neutrino mixing matrix elements in both of our benchmark scenarios are well within the 1σ interval of the current global fit values from 3-neutrino oscillation data [2]:

$$|V| = \begin{pmatrix} 0.795 - 0.846 & 0.513 - 0.585 & 0.126 - 0.178 \\ 0.205 - 0.543 & 0.416 - 0.730 & 0.579 - 0.808 \\ 0.215 - 0.548 & 0.409 - 0.725 & 0.567 - 0.800 \end{pmatrix}. \quad (22)$$

Note here that the constraints due to (22) are actually stronger than those obtained from (21).

We conclude this section by deriving a relationship between the general unitary matrix \mathcal{U}_6 that fully diagonalizes the effective neutrino mass matrix \mathcal{M}_{eff} in (10) and the unitary matrix \mathcal{V} introduced in (6) which only block-diagonalizes \mathcal{M}_{eff} as in (11). This relationship can be obtained by rewriting (A5) as follows:

$$\mathcal{U}_6 = \begin{pmatrix} \mathbf{1}_3 & \mathbf{0}_3 \\ \mathbf{0}_3 & U_0 \end{pmatrix} \begin{pmatrix} A & R \\ S & B \end{pmatrix} \begin{pmatrix} V_0 & \mathbf{0}_3 \\ \mathbf{0}_3 & \mathbf{1}_3 \end{pmatrix} = \mathcal{V} \begin{pmatrix} \mathbf{1}_3 & \mathbf{0}_3 \\ \mathbf{0}_3 & U_0 \end{pmatrix} \begin{pmatrix} V_0 & \mathbf{0}_3 \\ \mathbf{0}_3 & \mathbf{1}_3 \end{pmatrix}, \quad (23)$$

where \mathcal{V} is identified as

$$\mathcal{V} = \begin{pmatrix} \mathbf{1}_3 & \mathbf{0}_3 \\ \mathbf{0}_3 & U_0 \end{pmatrix} \begin{pmatrix} A & R \\ S & B \end{pmatrix} \begin{pmatrix} \mathbf{1}_3 & \mathbf{0}_3 \\ \mathbf{0}_3 & U_0^\dagger \end{pmatrix} \equiv \begin{pmatrix} \mathbf{1}_3 & \mathbf{0}_3 \\ \mathbf{0}_3 & U_0 \end{pmatrix} \tilde{\mathcal{V}} \begin{pmatrix} \mathbf{1}_3 & \mathbf{0}_3 \\ \mathbf{0}_3 & U_0^\dagger \end{pmatrix}, \quad (24)$$

and $\tilde{\mathcal{V}}$ has an exact representation as in (6) with the replacement $\zeta \rightarrow \tilde{\zeta} = \zeta U_0^*$.

V. BENCHMARK SCENARIOS FOR LIGHT AND SUPERLIGHT STERILE NEUTRINOS

In this section, we consider two physically interesting benchmark scenarios as shown in Fig. 4 and comment on a third one considered recently in the literature. We develop a method which enables us to fit some of the model parameters for each benchmark scenario, so as to be compatible with the SBL data. It also allows us to determine the values for the remaining theoretical parameters that have not yet been constrained by the existing neutrino data and could be probed in future experiments.

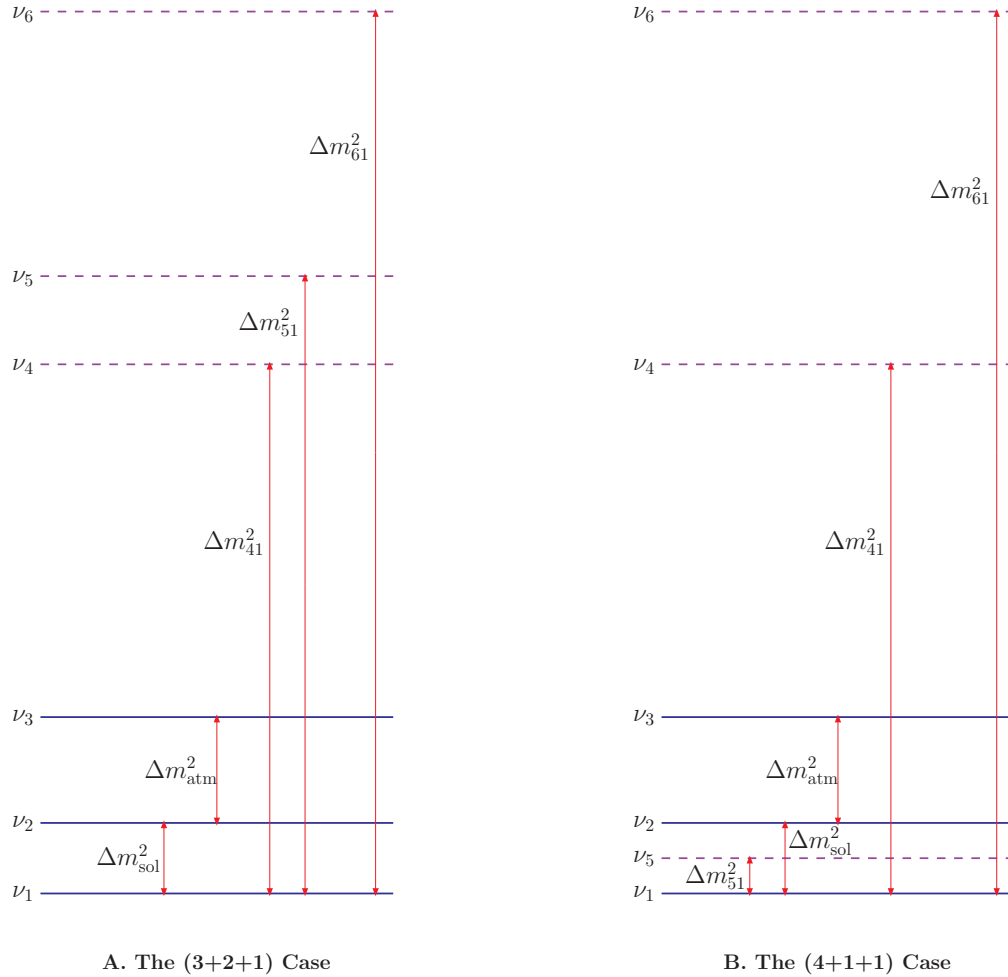


FIG. 4: The two benchmark scenarios discussed in Sections V A and V B. The solid (dashed) horizontal lines represent the mostly active (sterile) neutrino mass eigenstates. The masses are not to scale.

Employing the block form of \mathcal{U}_6 in (A5), we obtain from (16) the following consistency conditions on the model parameters M_D , M_N and μ_R :

$$\tilde{R}^* \widehat{M}_{123} \tilde{R}^\dagger + U^* \widehat{M}_{456} U^\dagger = M_N \mu_R^{-1} M_N^\top, \quad (25)$$

$$V^* \widehat{M}_{123} \tilde{R}^\dagger + R^* \widehat{M}_{456} U^\dagger = M_D \mu_R^{-1} M_N^\top, \quad (26)$$

$$V^* \widehat{M}_{123} V^\dagger + R^* \widehat{M}_{456} R^\dagger = M_D \mu_R^{-1} \left(\mathbf{1}_3 + x_R f(x_R) \right) M_D^\top. \quad (27)$$

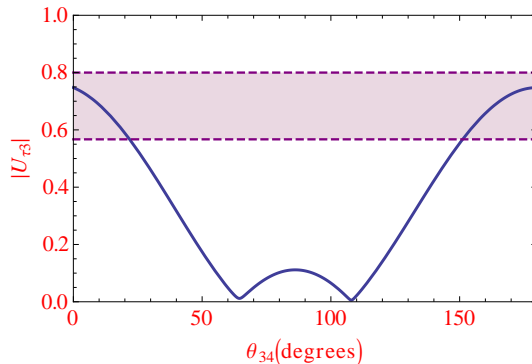


FIG. 5: The magnitude of the mixing element $U_{\tau 3}$ as a function of the mixing angle θ_{34} . The shaded region shows the experimentally allowed range.

Using the best-fit values for the mass and mixing parameters discussed in Section IV, we can derive constraints on the MRISM parameter space. For simplicity, we assume normal hierarchy⁴ for the active neutrinos, i.e., $m_1 < m_2 \ll m_3$, with $m_1 = 0$.

A. The (3+2+1) Case

In this scenario, we assume that all three active neutrinos are lighter than the three light sterile neutrinos, as shown schematically in Fig. 4A. Among the three light sterile neutrinos, we assume one to be of order keV-scale to account for a warm/cold DM candidate and/or pulsar kicks [49]. Following the analysis of [50], we take the largest mass eigenvalue to be $m_6 = 1$ keV and the mixing parameters $|U_{\alpha 6}| = 7 \times 10^{-3}$, for $\alpha = e, \mu, \tau$, which implies the mixing angles $\theta_{i6} = 0.4^\circ$, for $i = 1, 2, 3$ in (A5). We also choose $\varphi_{i6} = 0$ for $i = 1, 2, 3, 4$ since these phases do not affect the SBL data significantly. The other two light sterile neutrinos are assumed to have eV-scale masses in order to explain the LSND+MiniBooNE results and reactor anomalies [10–14]. Thus we have a simple extension of the (3+2)-models discussed in the literature which can now account for the DM as well.

Since the third sterile state is much heavier than the other two and its mixing effects are very small, we can still use the global analysis of the (3+2)-scenario. From the latest global fit of [13] including the most recent MiniBooNE data⁵, we get the best-fit values of $\Delta m_{41}^2 = 0.92$ eV², $\Delta m_{51}^2 = 17$ eV², and

$$|U_{e4}| = 0.15, \quad |U_{\mu 4}| = 0.13, \quad |U_{e5}| = 0.069, \quad |U_{\mu 5}| = 0.16, \quad \phi_{54} \equiv \arg(U_{e5}U_{\mu 5}^*U_{e4}^*U_{\mu 4}) = 1.8\pi, \quad (28)$$

which imply

$$\theta_{15} = 4.0^\circ, \quad \theta_{25} = 9.2^\circ, \quad \theta_{14} = 8.6^\circ, \quad \theta_{24} = 7.7^\circ, \quad \phi_{54} \simeq (\varphi_{14} - \varphi_{24}) + (\varphi_{25} - \varphi_{15}) = 1.8\pi. \quad (29)$$

Note that the only experimentally relevant CP -phase in the (3+2)-case is the combination ϕ_{54} , which enters the $\bar{\nu}_\mu \rightarrow \bar{\nu}_e$ transition probability. Thus, we cannot determine all the 5 Dirac phases in the (3+2)-sector. We assume for simplicity that the Dirac phases $\varphi_{24}, \varphi_{15}, \varphi_{25}, \varphi_{35}$ are all zero⁶ so that $\phi_{54} \simeq \varphi_{14}$. We also take the mixing angles θ_{34} and θ_{35} to be equal which can now be constrained from the allowed range of values for $|U_{\tau 3}|$ since in the

⁴ The case of inverted hierarchy can be worked out in a similar way. For a discussion of all possible scenarios with two and three sterile neutrinos, see [48].

⁵ The allowed region in the $\Delta m_{41}^2 - \Delta m_{51}^2$ plane from the global fit of [13] is somewhat different from the other recent global fits [10–12, 14]. This is mainly because the disappearance data sets used in [13] prefer a medium Δm_{41}^2 (0.92 eV²) and a high Δm_{51}^2 (18 eV²) whereas the appearance data sets prefer a low Δm_{41}^2 (0.31 eV²) and a medium Δm_{51}^2 (1.0 eV²). This incompatibility is expected to be addressed soon after more MiniBooNE neutrino data become available.

⁶ We find that allowing a nonzero value for any of these phases does not change our fit significantly.

PMNS parametrization this element depends *only* on the mixing angles θ_{23} and θ_{13} , whose values are now known experimentally [1]. This is shown in Fig. 5, where we plot the dependence of $|U_{\tau 3}|$ on $\theta_{34} = \theta_{35}$. The allowed range of $|U_{\tau 3}|$ as given in (22) is shown as the shaded region. Thus, we see that in the first quadrant only $\theta_{34} < 22.1^\circ$ is allowed.

While θ_{34} and θ_{45} are constrained to be small as shown in Fig. 5, the other three mixing angles, viz. θ_{45}, θ_{46} and θ_{56} , parametrizing the mixing effects in the purely sterile sector are mostly insensitive to oscillation experiments. However, using the consistency conditions for our model parameters given by (25)–(27), we can *predict* their best-fit values along with the model parameters satisfying these conditions.

Our approach to data fitting may be described as follows. For a given set of values for the mixing angles $\{\theta_{34}, \theta_{35}, \theta_{45}, \theta_{46}, \theta_{56}\}$ and the scale $\hat{\mu}_R$, we solve for the mass matrix M_N exactly using (25) for a symmetric structure of M_N , i.e., for $M_N = M_N^T$. Then using (26), we obtain the input values for the elements of the mass matrix M_D , which we use to check the validity of (27). More precisely, we minimize the dimensionless function

$$\mathcal{F} = \frac{\left\| \left(V^* \widehat{M}_{123} V^\dagger + R^* \widehat{M}_{456} R^\dagger \right) - \left[M_D \mu_R^{-1} \left(\mathbf{1}_3 + x_R f(x_R) \right) M_D^T \right] \right\|}{\left\| V^* \widehat{M}_{123} V^\dagger + R^* \widehat{M}_{456} R^\dagger \right\|}, \quad (30)$$

with respect to the set of variables $\{\theta_{34}, \theta_{35}, \theta_{45}, \theta_{46}, \theta_{56}\}$ while requiring that the elements $U_{\tau i}$ for $i = 1, 2, 3$ lie within the allowed range given in (22). For illustration, our results for $x_R = 1$ case are shown in Fig. 6 and the best-fit values of the mixing angles that minimize the function \mathcal{F} given by (30) are

$$\theta_{34} = 0.1^\circ, \quad \theta_{35} = 19.6^\circ, \quad \theta_{45} = 26.4^\circ, \quad \theta_{46} = 12.9^\circ, \quad \theta_{56} = 54.8^\circ, \quad (31)$$

which yields for the active neutrino mixing matrix

$$|V| = \begin{pmatrix} 0.8150 & 0.5354 & 0.1475 \\ 0.4793 & 0.5881 & 0.6182 \\ 0.3032 & 0.5826 & 0.6783 \end{pmatrix}, \quad (32)$$

and the model parameter values

$$M_D = \begin{pmatrix} 0.0605 - 0.0210i & 0.0529 + 0.0105i & 0.0127 - 0.0066i \\ 0.0839 + 0.0002i & 0.0743 & -0.0270 - 0.0001i \\ 0.0941 + 0.0003i & 0.1321 - 0.0002i & -0.1131 + 0.0001i \end{pmatrix} \text{ MeV}, \quad (33)$$

$$M_N = \begin{pmatrix} 0.7508 + 0.0004i & 1.5916 + 0.0001i & 0.9986 - 0.0003i \\ 1.5916 + 0.0001i & 5.8432 - 0.0002i & 3.7990 + 0.0002i \\ 0.9986 - 0.0003i & 3.7990 + 0.0002i & 3.1780 - 0.0002i \end{pmatrix} \text{ MeV}. \quad (34)$$

with $\|\zeta\| = 0.44$. Note that this leads to a very small non-unitary effect due to the mixing of the active neutrinos with the heavy sterile states: $\|M_D \mu_R^{-1}\| \sim 10^{-9}$. On the other hand, the non-unitarity due to the mixing with the light sterile states is well within the 1σ uncertainty in the active neutrino mixing matrix, as can be seen by comparing (22) with (32).

B. The (4+1+1) Case

In this case, we assume that one of the sterile neutrinos is in the keV-range to account for the DM as in the previous case. Another sterile state is assumed to be in the eV-range to explain the SBL data. Thus, this can be regarded as a simple extension of the (3+1)-models discussed in the literature. The third sterile state is superlight (well below the eV range), having a weak mixing to the active sector, so that it does not contribute much to the SBL data. This scenario is shown schematically in Fig. 4B. To the best of our knowledge, an explicit model with such a superlight sterile neutrino in the vicinity of the active neutrinos while being consistent with the SBL data has not been considered in the literature so far. Here, we would like to explore such a possibility and its experimental prospects.

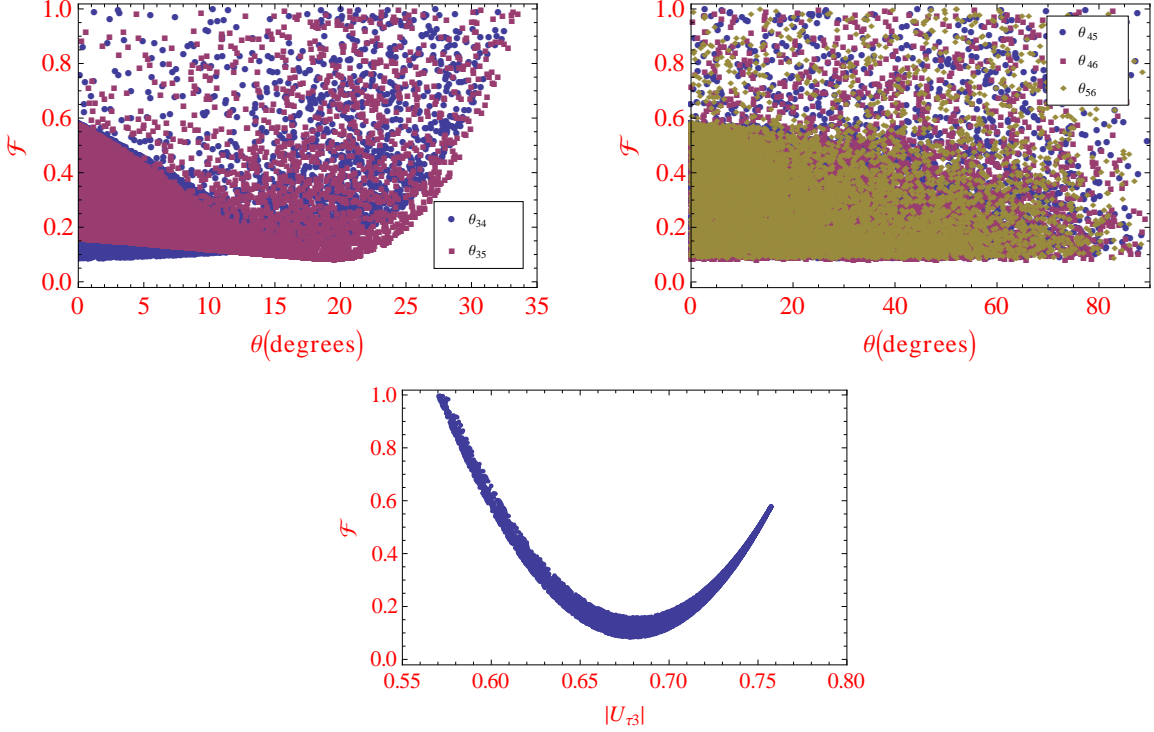


FIG. 6: The function \mathcal{F} defined in (30) versus the active-sterile neutrino mixing parameters for the (3+2+1) case.

A superlight sterile state in the vicinity of the electron neutrino was considered in [51] with $\Delta m_{61}^2 \sim (0.2 - 2) \times 10^{-5} \text{ eV}^2$ and the mixing angle $\sin^2 2\theta_{16} \sim 10^{-3}$ in order to explain the absence of an upturn at low energies in the solar neutrino data. They also required the mixing $|U_{s33}|^2 \sim 0.02 - 0.2$ in order to have a significant production of this superlight sterile state in the early Universe, which could generate the additional effective relativistic degree of freedom, $\Delta N_{\text{eff}} \sim 1$ as observed from the recent Wilkinson Microwave Anisotropy Probe (WMAP) data [15]⁷, provided the mixing is large: $|U_{s33}|^2 \sim 0.1 - 0.2$. For illustration, let us consider a similar situation as in [51], with

$$\Delta m_{51}^2 = 2 \times 10^{-5} \text{ eV}^2, \quad \theta_{15} = \theta_{25} = 2.0^\circ, \quad (35)$$

while for the eV-scale sterile state, we use the best-fit value for the (3+1)-scenario [13]:

$$\Delta m_{41}^2 = 0.92 \text{ eV}^2, \quad |U_{e4}| = 0.15, \quad |U_{\mu 4}| = 0.17. \quad (36)$$

Also, we assume for simplicity that the Dirac phases $\varphi_{24}, \varphi_{15}, \varphi_{25}, \varphi_{35}, \varphi_{16}, \varphi_{26}, \varphi_{36}, \varphi_{46}$ are all zero. The allowed range of values for $|U_{\tau 3}|$ will then constrain the values of the mixing angles θ_{34}, θ_{35} and θ_{36} to be small. For $\theta_{34} = \theta_{35}$, this is shown in the left-panel of Fig. 7 where we have shown the allowed range of $\theta_{36} = [0, 2\pi/9]$. On the other hand, if we choose $\theta_{34} = \theta_{35} = \theta_{36}$, then the mixing angles are constrained to be $< 22.1^\circ$, as in the previous scenario. This is shown in the right panel of Fig. 7.

Using the consistency conditions for our model parameters given by (25)–(27), we can derive the best-fit values for the set of six mixing angles $\{\theta_{34}, \theta_{35}, \theta_{36}, \theta_{45}, \theta_{46}, \theta_{56}\}$, as well as the corresponding model parameter values. To achieve this, we minimize the function defined in (30) while simultaneously requiring that the elements $|U_{\tau i}|$ for $i = 1, 2, 3$ fall within the allowed range of $|V_{\tau 3}|$ given in (22). In addition, we require that the element $|U_{s33}|^2$ should

⁷ Note that in our case, the eV-scale sterile neutrino could also contribute to ΔN_{eff} , depending on its thermal history at the Big Bang Nucleosynthesis epoch.

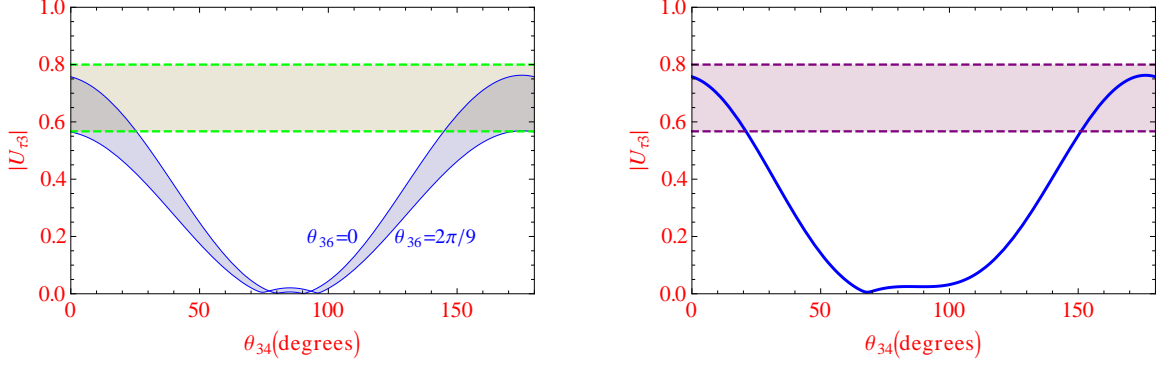


FIG. 7: The magnitude of the mixing element $U_{\tau 3}$ as a function of the mixing angle $\theta_{34} = \theta_{35}$ with θ_{36} as a free parameter (left panel) and with $\theta_{36} = \theta_{34}$ (right panel). The horizontal shaded region shows the experimentally allowed range.

be within $0.1 - 0.2$, as discussed above. For $x_R = 1$, our results are shown in Fig. 8 and the best-fit values for the mixing angles which minimize the function \mathcal{F} defined in (30) are

$$\theta_{34} = 10.6^\circ, \quad \theta_{35} = 10.8^\circ, \quad \theta_{36} = 23.8^\circ, \quad \theta_{45} = 82.3^\circ, \quad \theta_{46} = 1.0^\circ, \quad \theta_{56} = 50.8^\circ, \quad (37)$$

with $|U_{s33}|^2 = 0.16$ and

$$|V| = \begin{pmatrix} 0.8165 & 0.5364 & 0.1477 \\ 0.4788 & 0.5948 & 0.6221 \\ 0.2730 & 0.5498 & 0.6380 \end{pmatrix}. \quad (38)$$

The corresponding model parameters are

$$M_D = \begin{pmatrix} 0.0075 + 0.0021i & 0.2210 + 0.0154i & 0.2239 - 0.0188i \\ -0.0072 + 0.0002i & 0.2129 & 0.2337 \\ 0.0439 - 0.0002i & 2.76678 - 0.0001i & 2.3209 + 0.0002i \end{pmatrix} \text{ MeV}, \quad (39)$$

$$M_N = \begin{pmatrix} 0.0258 & 0.0910 & 0.1060 \\ 0.0910 & 5.0303 & 3.8820 \\ 0.1060 & 3.8820 & 3.4258 \end{pmatrix} \text{ MeV}. \quad (40)$$

with $\|\zeta\| = 1.45$. Again in this case, we find that the non-unitarity effects are small, as can be seen by comparing (22) with (38).

C. The (3+3) Case

Finally, we would like to comment on the case where all the three sterile neutrinos are in the eV-range and heavier than the active ones. It was shown in [13] that this scenario has the highest compatibility between the neutrino and anti-neutrino data sets, but still has a poor compatibility between the appearance and disappearance data sets. They obtained the following best-fit values for the experimentally relevant 12 parameters in the (3+3)-case:

$$\begin{aligned} \Delta m_{41}^2 &= 0.90 \text{ eV}^2, & \Delta m_{51}^2 &= 17 \text{ eV}^2, & \Delta m_{61}^2 &= 22 \text{ eV}^2, \\ |U_{\mu 4}| &= 0.12, & |U_{e 4}| &= 0.11, & |U_{\mu 5}| &= 0.17, & |U_{e 5}| &= 0.11, & |U_{\mu 6}| &= 0.14, & |U_{e 6}| &= 0.11, \\ \phi_{54} &\equiv \arg(U_{e5}U_{\mu 5}^*U_{e4}^*U_{\mu 4}) = 1.6\pi, & \phi_{64} &\equiv \arg(U_{e6}U_{\mu 6}^*U_{e4}^*U_{\mu 4}) = 0.28\pi, & \phi_{65} &\equiv \arg(U_{e6}U_{\mu 6}^*U_{e5}^*U_{\mu 5}) = 1.4\pi. \end{aligned} \quad (41)$$

For the parametrization of the unitary matrix discussed in Appendix A, this yields

$$\theta_{16} = 6.3^\circ, \quad \theta_{26} = 8.1^\circ, \quad \theta_{15} = 6.3^\circ, \quad \theta_{25} = 9.9^\circ, \quad \theta_{14} = 6.6^\circ, \quad \theta_{24} = 7.1^\circ, \quad (42)$$

$$\phi_{54} \simeq (\varphi_{14} - \varphi_{24}) + (\varphi_{25} - \varphi_{15}), \quad \phi_{64} \simeq (\varphi_{14} - \varphi_{24}) + (\varphi_{26} - \varphi_{16}), \quad \phi_{65} \simeq (\varphi_{15} - \varphi_{25}) + (\varphi_{26} - \varphi_{16}). \quad (43)$$

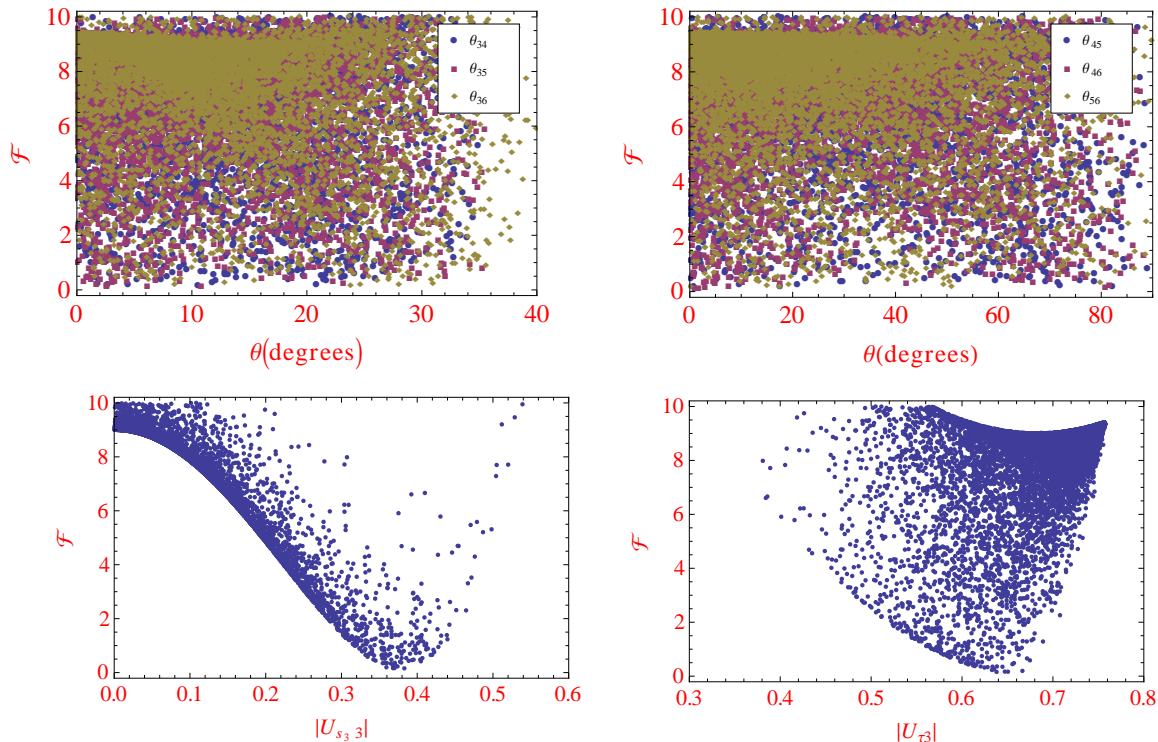


FIG. 8: The function \mathcal{F} defined in (30) versus the active-sterile mixing parameters for the (4+1+1) case.

Thus, we find that the three experimentally relevant Dirac CP phases for the (3+3) scenario are *not* independent of each other, and only two of them are independent, as already noted in [52]. Hence, we cannot obtain a solution for the phases in (43) satisfying the values given in (41), which were presumably obtained by assuming that they are independent parameters. Note that it is also very difficult to make the (3+3)-scenario with the best-fit Δm^2 values given by (41) compatible with a standard cosmological model.

VI. CONCLUSIONS

We have discussed the possibility of having light and superlight sterile neutrinos in the recently proposed Minimal Radiative Inverse Seesaw Model. In the limit $\|\mu_R\| \gg \|M_D\|, \|M_N\|$, after integrating out the heavy singlet states with masses of order $\|\mu_R\|$, we are left with three light sterile neutrinos along with the three usual active neutrinos. We have considered two benchmark scenarios for the mass hierarchy of these light sterile states. In the first scenario, denoted as the (3+2+1)-scenario, one of the light sterile states has mass in the keV-range and very small mixing with the active neutrinos to account for the Dark Matter in the Universe, whilst the other two sterile states are in the eV-range with non-zero mixing with the active states, as required to explain the LSND+MiniBooNE+reactor neutrino data.

In this article, we have also discussed another potentially interesting scenario, denoted as the (4+1+1)-scenario, with one superlight sterile neutrino state almost degenerate in mass with the solar neutrinos, within the context of the Minimal Radiative Inverse Seesaw Model. This superlight sterile neutrino may mix weakly with both solar and atmospheric neutrinos and might give rise to observable effects in the current and future neutrino data. Such superlight sterile neutrinos may also provide an explanation for the extra radiation observed in the Universe. Moreover, this scenario is more compatible with the cosmological constraints on the sum of the neutrino masses.

Finally, we note that both of these scenarios discussed here constitute *complete* extensions of the Standard Model

Since ω_{45} commutes with ω_{i6} for $i = 1, 2, 3$ [cf. (A2, A3)], we can rewrite (A4) as

$$\begin{aligned} \mathcal{U}_6 &= (\omega_{56}\omega_{46}\omega_{45})(\omega_{36}\omega_{26}\omega_{16}\omega_{35}\omega_{25}\omega_{15}\omega_{34}\omega_{24}\omega_{14})(\omega_{23}\omega_{13}\omega_{12}) \\ &= \begin{pmatrix} \mathbf{1}_3 & \mathbf{0}_3 \\ \mathbf{0}_3 & U_0 \end{pmatrix} \begin{pmatrix} A & R \\ S & B \end{pmatrix} \begin{pmatrix} V_0 & \mathbf{0}_3 \\ \mathbf{0}_3 & \mathbf{1}_3 \end{pmatrix} \equiv \begin{pmatrix} V & R \\ \tilde{R} & U \end{pmatrix}. \end{aligned} \quad (\text{A5})$$

Here the 3×3 unitary matrices U_0, V_0 involve the mixing *only* within purely sterile and purely active neutrinos respectively, whereas the matrices R, S are responsible for the active-sterile mixing. For convenience, we have defined

$$V \equiv AV_0, \quad U \equiv U_0B, \quad \tilde{R} \equiv U_0SV_0. \quad (\text{A6})$$

where V is the new Pontecorvo-Maki-Nakagawa-Sakata (PMNS) mixing matrix for the active neutrinos. The analytical form of the matrices in (A5), in terms of the mixing angles and phases, has been presented in [54].

Finally, we note that the unitarity of \mathcal{U}_6 implies:

$$\begin{aligned} VV^\dagger &= AA^\dagger = \mathbf{1}_3 - RR^\dagger, \\ U^\dagger U &= B^\dagger B = \mathbf{1}_3 - R^\dagger R. \end{aligned} \quad (\text{A7})$$

Thus, the matrix R measures the non-unitarity of the PMNS matrix V .

- [1] For a review, see, e.g. K. Nakamura and S. T. Petcov, in J. Beringer *et al.* (Particle Data Group), Phys. Rev. **D86**, 010001 (2012) (<http://pdg.lbl.gov>).
- [2] M. C. Gonzalez-Garcia, M. Maltoni, J. Salvado and T. Schwetz, arXiv:1209.3023 [hep-ph].
- [3] For other recent global fits to the 3-neutrino oscillation data, see D. V. Forero, M. Tortola and J. W. F. Valle, Phys. Rev. D **86**, 073012 (2012) [arXiv:1205.4018 [hep-ph]]; G. L. Fogli, E. Lisi, A. Marrone, D. Montanino, A. Palazzo and A. M. Rotunno, Phys. Rev. D **86**, 013012 (2012) [arXiv:1205.5254 [hep-ph]].
- [4] A. Aguilar-Arevalo *et al.* [LSND Collaboration], Phys. Rev. D **64**, 112007 (2001) [hep-ex/0104049].
- [5] A. A. Aguilar-Arevalo *et al.* [MiniBooNE Collaboration], Phys. Rev. Lett. **105**, 181801 (2010) [arXiv:1007.1150 [hep-ex]]; A. A. Aguilar-Arevalo *et al.* [MiniBooNE Collaboration], arXiv:1207.4809 [hep-ex].
- [6] G. Mention *et al.*, Phys. Rev. D **83**, 073006 (2011) [arXiv:1101.2755 [hep-ex]].
- [7] <http://lepewwg.web.cern.ch/LEPEWWG/>.
- [8] For a recent review, see, K. N. Abazajian *et al.*, arXiv:1204.5379 [hep-ph].
- [9] T. A. Mueller *et al.*, Phys. Rev. C **83**, 054615 (2011) [arXiv:1101.2663 [hep-ex]].
- [10] J. Kopp, M. Maltoni and T. Schwetz, Phys. Rev. Lett. **107**, 091801 (2011) [arXiv:1103.4570 [hep-ph]].
- [11] C. Giunti and M. Laveder, Phys. Rev. D **84**, 073008 (2011) [arXiv:1107.1452 [hep-ph]].
- [12] A. Donini, P. Hernandez, J. Lopez-Pavon, M. Maltoni and T. Schwetz, JHEP **1207**, 161 (2012) [arXiv:1205.5230 [hep-ph]].
- [13] J. M. Conrad, C. M. Ignarra, G. Karagiorgi, M. H. Shaevitz and J. Spitz, arXiv:1207.4765 [hep-ex].
- [14] M. Archidiacono, N. Fornengo, C. Giunti and A. Melchiorri, Phys. Rev. D **86**, 065028 (2012) [arXiv:1207.6515 [astro-ph.CO]].
- [15] E. Komatsu *et al.* [WMAP Collaboration], Astrophys. J. Suppl. **192**, 18 (2011) [arXiv:1001.4538 [astro-ph.CO]].
- [16] J. Hamann, S. Hannestad, G. G. Raffelt, I. Tamborra and Y. Y. Y. Wong, Phys. Rev. Lett. **105**, 181301 (2010) [arXiv:1006.5276 [hep-ph]]; J. Hamann, S. Hannestad, G. G. Raffelt and Y. Y. Y. Wong, JCAP **1109**, 034 (2011) [arXiv:1108.4136 [astro-ph.CO]]. See also, S. Joudaki, K. N. Abazajian and M. Kaplinghat, arXiv:1208.4354 [astro-ph.CO].
- [17] N. E. Mavroumatos and A. Pilaftsis, arXiv:1209.6387 [hep-ph].
- [18] P. Minkowski, Phys. Lett. **B67**, 421 (1977); T. Yanagida, in *Workshop on Unified Theories*, KEK Report 79-18, p. 95 (1979); M. Gell-Mann, P. Ramond and R. Slansky, in *Supergravity*, P. van Nieuwenhuizen and D. Z. Freedman (eds.), North Holland, Amsterdam (1979), p. 315; S. L. Glashow, in *1979 Cargese Summer Institute on Quarks and Leptons*, M. Levy *et al.* (eds.), Plenum Press, New York (1980), p.687; R. N. Mohapatra and G. Senjanovic, Phys. Rev. Lett. **44**, 912 (1980); J. Schechter and J. W. F. Valle, Phys. Rev. D **22**, 2227 (1980).
- [19] A. de Gouvea, Phys. Rev. D **72**, 033005 (2005) [hep-ph/0501039].
- [20] A. de Gouvea, W. -C. Huang and J. Jenkins, Phys. Rev. D **80**, 073007 (2009) [arXiv:0906.1611 [hep-ph]].
- [21] R. N. Mohapatra, Phys. Rev. Lett. **56**, 561 (1986); R. N. Mohapatra and J. W. F. Valle, Phys. Rev. **D34**, 1642 (1986).
- [22] R. N. Mohapatra, S. Nasri and H. -B. Yu, Phys. Rev. D **72**, 033007 (2005) [hep-ph/0505021].
- [23] C. S. Fong, R. N. Mohapatra and I. Sung, Phys. Lett. B **704**, 171 (2011) [arXiv:1107.4086 [hep-ph]].
- [24] E. J. Chun, A. S. Joshipura and A. Y. Smirnov, Phys. Rev. D **54**, 4654 (1996) [hep-ph/9507371]; J. Barry, W. Rodejohann and H. Zhang, JHEP **1107**, 091 (2011) [arXiv:1105.3911 [hep-ph]]; H. Zhang, Phys. Lett. B **714**, 262 (2012) [arXiv:1110.6838 [hep-ph]]; J. Heeck and H. Zhang, arXiv:1211.0538 [hep-ph].

- [25] P. S. B. Dev and A. Pilaftsis, Phys. Rev. D **86**, 113001 (2012) [arXiv:1209.4051 [hep-ph]].
- [26] A. Pilaftsis, Z. Phys. C **55**, 275 (1992) [hep-ph/9901206].
- [27] T. Asaka, M. Shaposhnikov and A. Kusenko, Phys. Lett. B **638**, 401 (2006) [hep-ph/0602150].
- [28] J. G. Korner, A. Pilaftsis and K. Schilcher, Phys. Rev. D **47**, 1080 (1993) [hep-ph/9301289].
- [29] C. Giunti and M. Laveder, Phys. Rev. D **84**, 093006 (2011) [arXiv:1109.4033 [hep-ph]]; C. Giunti and M. Laveder, Phys. Lett. B **706**, 200 (2011) [arXiv:1111.1069 [hep-ph]]; G. Karagiorgi, M. H. Shaevitz and J. M. Conrad, arXiv:1202.1024 [hep-ph]; C. Giunti, M. Laveder, Y. F. Li, Q. Y. Liu and H. W. Long, arXiv:1210.5715 [hep-ph].
- [30] V. N. Aseev *et al.*, Phys. Atom. Nucl. **75**, 464 (2012) [Yad. Fiz. **75**, 500 (2012)].
- [31] C. Kraus *et al.*, Eur. Phys. J. C **40**, 447 (2005) [hep-ex/0412056].
- [32] C. Kraus, A. Singer, K. Valerius and C. Weinheimer, arXiv:1210.4194 [hep-ex].
- [33] See e.g., E. W. Otten and C. Weinheimer, Rept. Prog. Phys. **71**, 086201 (2008) [arXiv:0909.2104 [hep-ex]].
- [34] A. S. Riis and S. Hannestad, JCAP **1102**, 011 (2011) [arXiv:1008.1495 [astro-ph.CO]]; J. A. Formaggio and J. Barrett, Phys. Lett. B **706**, 68 (2011) [arXiv:1105.1326 [nucl-ex]]; A. Esmaili and O. L. G. Peres, Phys. Rev. D **85**, 117301 (2012) [arXiv:1203.2632 [hep-ph]].
- [35] H. V. Klapdor-Kleingrothaus *et al.*, Eur. Phys. J. A **12**, 147 (2001) [hep-ph/0103062].
- [36] C. Arnaboldi *et al.*, Phys. Rev. Lett. **95**, 142501 (2005) [hep-ex/0501034].
- [37] R. Arnold *et al.* [NEMO Collaboration], Phys. Rev. Lett. **95**, 182302 (2005) [hep-ex/0507083]; M. Bongrand [NEMO-3 Collaboration], arXiv:1105.2435 [hep-ex].
- [38] M. Auger *et al.* [EXO Collaboration], Phys. Rev. Lett. **109**, 032505 (2012) [arXiv:1205.5608 [hep-ex]].
- [39] W. Rodejohann, J. Phys. G **39**, 124008 (2012) [arXiv:1206.2560 [hep-ph]]; B. Schwingenheuer, arXiv:1210.7432 [hep-ex].
- [40] Y. F. Li and S. -s. Liu, Phys. Lett. B **706**, 406 (2012) [arXiv:1110.5795 [hep-ph]].
- [41] J. Lopez-Pavon, S. Pascoli and C. -f. Wong, arXiv:1209.5342 [hep-ph].
- [42] For a review, see e.g., J. Lesgourgues and S. Pastor, Phys. Rept. **429**, 307 (2006) [astro-ph/0603494].
- [43] M. C. Gonzalez-Garcia, M. Maltoni and J. Salvado, JHEP **1008**, 117 (2010) [arXiv:1006.3795 [hep-ph]]; E. Giusarma *et al.*, Phys. Rev. D **83**, 115023 (2011) [arXiv:1102.4774 [astro-ph.CO]]; S. Riemer-Sorensen, D. Parkinson, T. Davis and C. Blake, arXiv:1210.2131 [astro-ph.CO]; X. Wang *et al.*, JCAP **1211**, 018 (2012) [arXiv:1210.2136 [astro-ph.CO]]; E. Giusarma, R. de Putter and O. Mena, arXiv:1211.2154 [astro-ph.CO].
- [44] J. Hamann, S. Hannestad and Y. Y. Y. Wong, JCAP **1211**, 052 (2012) [arXiv:1209.1043 [astro-ph.CO]].
- [45] S. Antusch, C. Biggio, E. Fernandez-Martinez, M. B. Gavela and J. Lopez-Pavon, JHEP **0610**, 084 (2006) [hep-ph/0607020].
- [46] M. Malinsky, T. Ohlsson and H. Zhang, Phys. Rev. D **79**, 073009 (2009) [arXiv:0903.1961 [hep-ph]]; M. Malinsky, T. Ohlsson, Z. -z. Xing and H. Zhang, Phys. Lett. B **679**, 242 (2009) [arXiv:0905.2889 [hep-ph]]; P. S. B. Dev and R. N. Mohapatra, Phys. Rev. D **81**, 013001 (2010) [arXiv:0910.3924 [hep-ph]].
- [47] A. Abada, D. Das, A. M. Teixeira, A. Vicente and C. Weiland, arXiv:1211.3052 [hep-ph].
- [48] S. Goswami and W. Rodejohann, JHEP **0710**, 073 (2007) [arXiv:0706.1462 [hep-ph]].
- [49] For a review, see e.g., A. Kusenko, Phys. Rept. **481**, 1 (2009) [arXiv:0906.2968 [hep-ph]].
- [50] A. de Gouvea, J. Jenkins and N. Vasudevan, Phys. Rev. D **75**, 013003 (2007) [hep-ph/0608147].
- [51] P. C. de Holanda and A. Y. Smirnov, Phys. Rev. D **69**, 113002 (2004) [hep-ph/0307266]; Phys. Rev. D **83**, 113011 (2011) [arXiv:1012.5627 [hep-ph]].
- [52] M. Maltoni and T. Schwetz, Phys. Rev. D **76**, 093005 (2007) [arXiv:0705.0107 [hep-ph]].
- [53] H. Harari and M. Leurer, Phys. Lett. B **181**, 123 (1986).
- [54] Z. -z. Xing, Phys. Rev. D **85**, 013008 (2012) [arXiv:1110.0083 [hep-ph]].